A Simple Rate-Equation-Based Thermal VCSEL Model

P. V. Mena, *Member, IEEE,* J. J. Morikuni, *Member, IEEE,* S.-M. Kang, *Fellow, IEEE,* A. V. Harton, *Member, IEEE,* and K. W. Wyatt

***Abstract*—Motivated by the potentially large number of devices and simulations involved in optoelectronic system design, and the associated need for compact optoelectronic device models, we present a simple thermal model of vertical-cavity surface-emitting laser (VCSEL) light-current (LI) characteristics based on the laser rate equations and a thermal offset current. The model was implemented in conventional SPICE-like circuit simulators, including HSPICE, and used to simulate key features of VCSEL LI curves, namely, thermally dependent threshold current and output-power roll-over for a range of ambient temperatures. The use of the rate equations also allows simulation in other non-dc operating regimes. Our results compare favorably to experimental data from three devices reported in the literature.**

***Index Terms*— Rate equations, semiconductor lasers, thermal modeling, vertical-cavity surface-emitting lasers (VCSEL's).**

I. Introduction

VERTICAL-CAVITY surface-emitting lasers (VCSEL's) have attracted considerable interest in recent years due to their single-longitudinal-mode operation, circular output beams, suitability for monolithic two-dimensional (2-D) integration, and compatibility with on-wafer probe testing [1]. However, despite these advantages, they still exhibit a number of less desirable features, which, while present in edge-emitters, can be considerably more pronounced in VCSEL's. For example, multimode operation is possible due to the existence of higher-order transverse modes [2]. Carrier diffusion and spatial hole burning can also be a factor, further limiting a VCSEL's performance by contributing to mode competition [3] and secondary pulsations in the turn-off transient [4]. However, the most recognized limitation of a VCSEL's performance is its thermal behavior.

Due to their poor heat dissipation and the large resistance introduced by their distributed Bragg reflectors (DBR's) [5], typical VCSEL's undergo relatively severe heating, and consequently can exhibit strong thermally dependent behavior. For example, thermal lensing due to a device's spatial temperature profile can yield considerable differences between cw and pulsed operation, as well as alter the emission profile of the laser's optical modes [6]. The most important effect, however, is exhibited in a device's static LI characteristics. First, analogous to edge-emitters, VCSEL's exhibit temperature-dependent threshold current. Second, because device temperature increases with injection current, the output power eventually rolls over and begins to decrease, thereby limiting a device's maximum cw output [6].

Clearly, in order to effectively design optoelectronic applications incorporating VCSEL's, appropriate models are required which account for thermal effects, in particular the temperature-dependent threshold current and output-power rollover identified above. The majority of such models to date have been largely numerical in nature, making use of detailed multidimensional analysis for the description of VCSEL thermal behavior. For example, Nakwaski and Osinski have developed extensive two-dimensional models of thermal heating [7], while other researchers have incorporated finite-element analysis of thermal effects into their comprehensive VCSEL simulations [8]-[10]. While these models are accurate, they are also computationally intensive. This feature makes them unattractive for the computer-aided design of optoelectronic systems, which are typically composed of many photonic and electronic components. For example, multichannel optical links [11] and smart pixel systems [12] require one-dimensional (1-D) and 2-D VCSEL arrays. Furthermore, system design often requires a large number of simulations for design optimization and verification. For example, the design of drive circuitry for a VCSEL may require many iterations to determine optimal transistor topology and sizing. In these cases, less-complicated VCSEL models that can accurately describe a device's operating characteristics are essential. This situation is analogous to that from IC design, where the use of computationally intensive multidimensional device models would make the efficient development of million- or even hundred-transistor designs a practical impossibility. Thus, with regards to the development and proliferation of optoelectronic systems, the importance of efficient and compact models for VCSEL's and other devices cannot be stressed enough.

Models have been developed which can be used to simulate the static LI characteristics without resorting to complicated multidimensional analysis. Yu *et al.* utilized a thermal rate equation in conjunction with device-parameter temperature dependencies to augment a rate equation description of VCSEL's [13]. Similarly, Su *et al.* implemented a simplified static model which also makes use of temperature-dependent model parameters [14]. While these models are indeed simpler

Manuscript received April 27, 1998; revised February 8, 1999.

P. V. Mena and S.-M. Kang are with the Department of Electrical and Computer Engineering, Beckman Institute for Advanced Science and Technology, University of Illinois at Urbana-Champaign, Urbana, IL 61801 USA.

J. J. Morikuni, A. V. Harton, and K. W. Wyatt are with the Optical Interconnect Laboratory, Applied Simulation and Modeling Research, Corporate Research and Development, Motorola, Inc., Schaumburg, IL 60196 USA.

Publisher Item Identifier S 0733-8724(99)03819-0.

than their highly numerical alternatives, they still require a description of thermal-dependent mechanisms in the VCSEL, such as the gain. Unfortunately, while even simpler models of a more empirical nature have been applied to LI characteristics at individual ambient temperatures [5], [15], they are limited to dc simulation. Thus, to the best of our knowledge, there exists a need for a simple thermal VCSEL model which, in addition to modeling basic laser behavior under *both* dc and non-dc conditions, can inherently describe static LI characteristics over a range of ambient temperatures without resorting to detailed descriptions of the thermal physics. Such semi-empirical models would significantly simplify the optoelectronic system-design process.

Based on the above observations, the development of such a VCSEL model should focus on two important considerations. First, the model should replicate the thermally dependent threshold current and output-power rollover seen in actual VCSEL's by using an empirical, rather than physical, description of the thermal mechanisms in the device. The model could then be used to study the thermal limitations placed on an optoelectronic design by the use of VCSEL's. Second, as noted above, the model must be able to simulate a VCSEL's non-dc behavior, namely small-signal and transient modulation. Obviously, the use of an empirical approach for modeling a VCSEL's thermal behavior will limit the range of validity over which such simulations can be performed. However, as we shall shortly discuss, this kind of model can simulate non-dc behavior over a typical range of operating conditions.

In this paper, we present a VCSEL model, based on the standard laser rate equations, that meets the above requirements. By introducing a thermally dependent empirical offset current into the rate equations, we are able to model in a simple manner the temperature-dependent threshold current and output power roll-over at different ambient temperatures, while retaining the ability to simulate ac and transient behavior as well. After discussing in Section II the basis for our model and its implementation in conventional SPICE-like simulators, we present in Section III comparisons of simulation to measured data for three devices reported in the literature. Final conclusions are presented in Section IV.

II. Model Development

The strong thermal dependence of VCSEL's can be attributed to a number of mechanisms. While Auger recombination [16] and optical losses such as intervalence band absorption [17] can play a role in the thermal behavior, the majority of effects during static, or cw, operation are due to the temperature-dependent laser gain and carrier leakage out of the active region.

First, as its temperature increases, a VCSEL's gain spectrum broadens and its peak location shifts to longer wavelengths. The device's emission wavelength also increases with temperature, though considerably less than the gain peak [18]. Consequently, depending on the initial location of the gain peak relative to the wavelength, the laser gain will either decrease or increase with temperature as the gain peak and wavelength become more or less mismatched [18]. In fact, an optimal value of temperature should exist in which the mismatch is eliminated to achieve a minimum threshold gain, as has been observed experimentally [18].

Second, thermal leakage of carriers out of the active region can lead to a reduction of injection efficiency which contributes to a VCSEL's thermal roll-over [19]. As the device temperature rises, the position of the active-layer's Fermi levels increases relative to the bandgap. Consequently, the active-layer becomes increasingly incapable of confining carriers. The resulting leakage can be modeled as a function of carrier density and temperature [19]. Because of the carrier-density dependence, spatial hole burning can result in further reduction of the injection efficiency [19].

All of these mechanisms affect the static LI characteristics by essentially making a VCSEL's differential efficiency and threshold current functions of temperature and carrier density. Thus, we could model a VCSEL's above-threshold LI curves using $P_o = \eta(T)(I - I_{\rm th}(N,T))$, where P_o is the optical output power, I is the injection current, $\eta(T)$ is the temperature-dependent differential slope efficiency, and $I_{\rm th}(N,T)$ is the threshold current as a function of carrier number N and temperature T [19]. To simplify this expression, we first assume that the slope efficiency's temperature-dependence has a minimal impact on the output [8]. Furthermore, by neglecting the effects of spatial hole burning [14], we can assume that the threshold current is solely a function of temperature. Thus, we can describe LI curves over a range of ambient temperatures using a constant slope efficiency and a temperature-dependent threshold current [6]. This approach is analogous to the one taken in modeling edge-emitters, where the threshold current is proportional to $\exp(T/T_o)$ and T_o is the characteristic temperature [20]. However, as discussed above, in VCSEL's the temperature-dependence is not simply an increasing function of temperature.

We could account for this dependence by describing key VCSEL parameters themselves as functions of temperature, in particular the laser gain [13], [21]. However, this approach requires a description of the thermal physics in the device. Because we want a simple model which avoids such details, we instead opt to partition the thermal threshold current into a constant value of threshold current $I_{\rm tho}$ plus an empirical thermal offset current $I_{\rm off}(T)$. This results in the expression

$$P_o = \eta(I - I_{\rm tho} - I_{\rm off}(T)). \tag{1}$$

All static thermal effects are now accounted for via the offset current, thereby circumventing the need for a more detailed approach. For simplicity, we choose to model this offset current using a polynomial function of temperature

$$I_{\rm off}(T) = a_0 + a_1 T + a_2 T^2 + a_3 T^3 + a_4 T^4 + \cdots \tag{2}$$

where the coefficients a_0–a_4 can be determined during parameter extraction. Because (2) is not exclusively an increasing function of temperature, it should be able to capture the general temperature dependency of a VCSEL's LI curves. For the devices discussed in Section III, we found that five terms were sufficient for implementing (2). However, at the expense of model complexity, additional terms can be added as necessary

if they help improve the accuracy of fitting the model to experimental data. It should also be noted that because the use of (1) and (2) results in the implicit fitting of the threshold current $I_{\rm th}(T)$ to the expression $I_{\rm tho}+I_{\rm off}(T)$, there appears to be a redundancy in the terms $I_{\rm tho}$ and a_0. However, in some cases the fit of $I_{\rm th}(T)$ results in extremely small or even negative values for the sum $I_{\rm tho}+a_0$. Clearly, if a_0 is set equal to zero, $I_{\rm tho}$ would have to take on this value. Therefore, to avoid this difficulty and allow $I_{\rm tho}$ to take on a more realistic value, we have included a_0 in (2).

Certainly, (1) and (2) could be used to directly simulate a VCSEL's LI characteristics, an approach that essentially amounts to a simple curve fit. However, like earlier empirical models [5], [15] which only focus on dc behavior, this approach would not permit small-signal and transient simulation of VCSEL's, critical elements of optoelectronic system design. Fortunately, it is well known that the simple above-threshold LI curve described by $P_o=\eta(I-I_{\rm th})$ can be described using the standard laser rate equations [20]. Thus, by introducing the offset current into these rate equations through an empirical fit to experimental data, we will be able to model LI curves at different temperatures as well as take advantage of many of the desirable properties of the rate equations, in particular the ability to model non-dc behavior such as small-signal modulation. Furthermore, because the rate equations are a widely accepted tool for modeling semiconductor lasers, we are confident that they serve as an efficient description of the basic lasing behavior of a wide variety of VCSEL's. Thus, the introduction of an empirical description of thermal behavior into this basic formulation should retain much of its general applicability, as suggested by the comparison with experimental data in Section III.

After the addition of the offset current, the modified rate equations are

$$\frac{dN}{dt}=\frac{\eta_i(I-I_{\rm off}(T))}{q}-\frac{N}{\tau_n}-\frac{G_o(N-N_o)S}{1+\varepsilon S} \tag{3}$$

$$\frac{dS}{dt}=-\frac{S}{\tau_p}+\frac{\beta N}{\tau_n}+\frac{G_o(N-N_o)S}{1+\varepsilon S} \tag{4}$$

where S is the photon number, η_i is the injection efficiency, τ_n is the carrier recombination lifetime, G_o is the gain coefficient, N_o is the carrier transparency number, τ_p is the photon lifetime, β is the spontaneous emission coupling coefficient, and ε is the gain-compression factor. The optical output power can be described using $P_o=kS$, where k is a scaling factor accounting for the output coupling efficiency of the VCSEL. These equations, along with (2), comprise the bulk of our model.

As we will shortly see, despite its simplicity, the introduction of the offset current into the rate equations is an extremely effective means for describing the thermal dependence of a VCSEL's continuous wave (CW) LI characteristics. Furthermore, the model should be able to simulate non-dc behavior in cases where the detailed thermal physics have a minimal impact on device modulation. In some cases, however, the thermal physics must be properly taken into account, and a more comprehensive physical model may then be necessary for describing the non-dc modulation of a VCSEL. For example, at elevated temperatures such as those found near or beyond the thermal rollover point in the LI curves, the thermal dependence of the gain and other internal parameters will have an important impact on a VCSEL's operating point. Significant modulation of the device temperature can have a similar effect on a device's thermally dependent mechanisms. Nonetheless, in many cases a VCSEL will be operated at currents well below the rollover point, where the effects of temperature can be minimized by avoiding significant thermal modulation of parameters such as the gain; in such cases, our model can be used to describe a VCSEL's non-dc behavior. For example, as suggested in the introduction, the thermal behavior of VCSEL's is typically an undesirable feature which should be minimized in the interests of a particular design. Consequently, a designer may wish to use our model in the simulation of a VCSEL-based application in order to determine the thermal limitations of that design's dc performance. Once a suitable operating point has been identified where thermal behavior is minimized, our model can then be used to simulate the design's non-dc operation. As we shall see in Section III, our model is indeed capable of simulating a VCSEL's small-signal modulation under these conditions, a fact which should make the model an attractive tool for optoelectronic system designers.

To complete the model, we still require expressions for the temperature and current-voltage characteristics of a VCSEL. First, while it is certainly possible to adopt detailed numerical representations of the VCSEL temperature profile as a function of the heat dissipation throughout the device [30], a much simpler method is to describe the temperature via a thermal rate equation which accounts for the transient temperature increase as a result of heat dissipation [13], [16]. Following this approach, we use

$$T=T_o+(IV-P_o)R_{\rm th}-\tau_{\rm th}\frac{dT}{dt} \tag{5}$$

where $R_{\rm th}$ is the VCSEL's thermal impedance (which relates the change in device temperature to the power dissipated as heat), $\tau_{\rm th}$ is a thermal time constant (which is necessary to account for the nonzero response time of the device temperature, observed to be on the order of 1 μs [6]), T_o is the ambient temperature, and V is the laser voltage. Under dc conditions, the dT/dt term disappears; thus, from the resulting equation it is clear that $(IV-P_o)$ models the power dissipated in the VCSEL, where we assume that any power not carried in the optical output is dissipated as heat in the device.

The current-voltage (IV) relationship, meanwhile, can be modeled in great detail based on the diode-like character of the VCSEL. However, for simplicity we have elected to represent the voltage across the device as an arbitrary empirical function of current and temperature using

$$V=f(I,T). \tag{6}$$

By introducing a capacitor or other parasitic components in parallel with this voltage, we can account for the complete electrical characteristics of the VCSEL (in which case (5) should be modified such that it depends on the total device current, not I). The advantage of this approach is that the

specific form of (6) can be determined on a device-by-device basis. For example, in some cases, a relationship which accounts for a resistance in series with a diode may be most appropriate, such as

$$V = IR_s + V_T \ln\left(1 + \frac{I}{I_s}\right) \tag{7}$$

where R_s is the series resistance, V_T is the diode's thermal voltage, and I_s is the diode's saturation current. In general, V_T is a function of temperature. However, when IV data is only available at one temperature, a constant value can be used. In other cases, a polynomial function of current and temperature [19] such as

$$V = (b_0 + b_1 T + b_2 T^2 + \cdots) \cdot (c_0 + c_1 I + c_2 I^2 + \cdots) \tag{8}$$

may work better, where b_0–b_2 and c_0–c_2 are constants. Additional terms can be included as needed. If we use experimental IV data to help determine all of the other model parameters first, then the exact form of (6) can be determined at the very end of parameter extraction for a specific device. While (8) could be used as a generic expression for any voltage data, a more compact expression such as (7) should be used when possible. This simplified approach not only allows the voltage's current and temperature dependence to be accurately modeled, but also permits the optical and electrical device characteristics to be largely decoupled from one another, thereby simplifying the extraction of model parameter values from experimental data.

Because one of our goals was to be able to use our model in the computer-aided design of optoelectronic systems, we have implemented (2)–(6) in a number of SPICE-like simulators, including Meta-Software's HSPICE [22] and Analogy's Saber [23]. As desired, this approach permits VCSEL's to be simulated in conjunction with electronic components, such as laser drivers, and other optoelectronic devices for which circuit-level models already exist. The HSPICE implementation relies on transformation of the model equations into an equivalent subcircuit representation as described in [24] and [29]. First, in order to improve the convergence properties of the model during simulation, we transformed P_o into a new variable v_m via $P_o = (v_m+\delta)^2$, and N into v_n via $N = z_n v_n$, where δ and z_n are arbitrary constants. Because of the nonlinear character and multiple solution regimes of the rate equations, such transformations help the simulator converge to a correct numerical solution [24]. After substituting these transformations into (2)–(6) and applying appropriate manipulations, we obtained the equivalent circuit illustrated in Fig. 1, where pd and nd are the electrical terminals of the VCSEL, po is the terminal whose node voltage models the output power P_o, and td is the terminal which models the device temperature T. Electrical characteristics are modeled via the nonlinear voltage source E_d, which implements (6), and the capacitor C_l, which models a simple parasitic shunting capacitance. Other parasitics can be added as necessary. The temperature equation (5) is modeled via the resistance $R_{\rm th}$, the capacitor $C_{\rm th} = \tau_{\rm th}/R_{\rm th}$, and the nonlinear current source $G_{\rm th}$ where [16]

$$G_{\rm th} = \frac{T_o}{R_{\rm th}} + (I_{\rm tot} V - P_o) \tag{9}$$

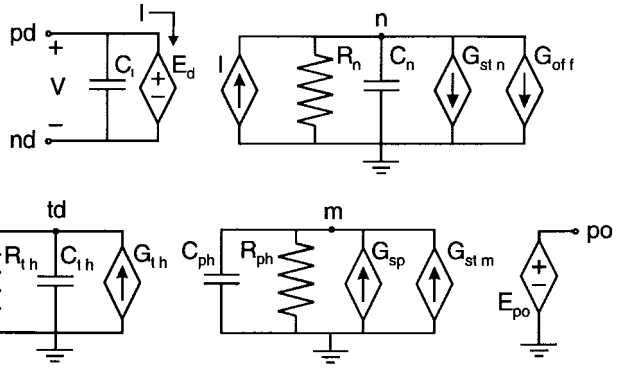

Fig. 1. Equivalent-circuit representation of simple thermal VCSEL model.

and $I_{\rm tot} = I + I_{Cl}$ is the total VCSEL current, with I_{Cl} accounting for current through C_l. The capacitor $C_n = qz_n/\eta_i$, resistor $R_n = \eta_i \tau_n/(qz_n)$, and nonlinear current sources $G_{\rm stn}$ and $G_{\rm off}$ implement the carrier rate equation (3), where

$$G_{\rm stn} = \frac{qG_o}{\eta_i k} \frac{(z_n v_n - N_o)(v_m+\delta)^2}{1 + \frac{\varepsilon}{k}(v_m+\delta)^2} \tag{10}$$

and $G_{\rm off}$ models the offset current from (2). Meanwhile, the capacitor $C_{\rm ph} = 2\tau_p$, resistor $R_{\rm ph} = 1$, and current sources $G_{\rm sp}$ and $G_{\rm stm}$ implement the photon rate equation (4) where

$$G_{\rm sp} = \frac{\tau_p \beta k z_n v_n}{\tau_n (v_m+\delta)} \tag{11}$$

$$G_{\rm stm} = \frac{G_o \tau_p (z_n v_n - N_o)(v_m+\delta)}{1 + \frac{\varepsilon}{k}(v_m+\delta)^2} - \delta. \tag{12}$$

Finally, $E_{\rm pf}$ transforms v_m into the output power P_o.

III. Comparison to Experiment

In order to use our model, we must be able to perform parameter extraction from measured data. If we substitute (5) into (1) under dc conditions, we obtain the expression

$$P_o = \eta[I - I_{\rm tho} - I_{\rm off}(T_o + (IV - P_o)R_{\rm th})]. \tag{13}$$

Using experimental LI and IV curves (i.e., experimental values for P_o, I, and V), we can optimize (13) to determine good initial values for $\eta, R_{\rm th}$, and the coefficients a_0–a_4 that will replicate the experimental LI data at various ambient temperatures T_o. This approach allows the thermal effects to be extracted without any knowledge of the thermal physics at work in the device. The complete set of model parameters can then be determined via additional parameter fitting; in other words, parameter optimization software can be used to determine an optimal set of model parameter values for matching simulated and experimental data. Finally, parameter-optimization software can also be used to determine the best form for the empirical expression (6), based on experimental values for I, V, and P_o, as well as the temperature T as calculated by (5). Below we discuss the application of our model to three different devices reported in the literature. Parameter optimization was performed using CFSQP [25].

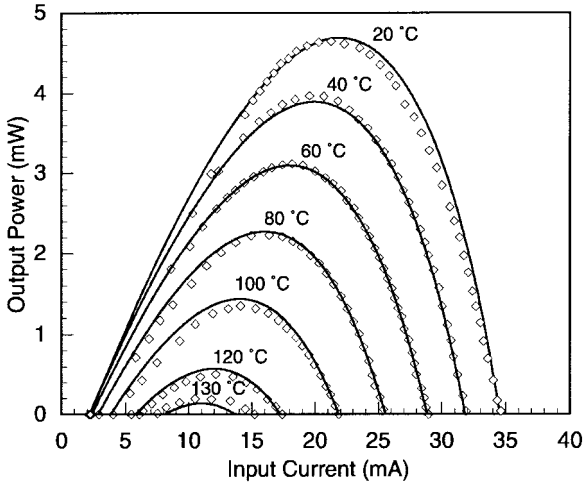

Fig. 2. Comparison of measured (data points) and simulated (lines) LI curves for a bottom-emitting 863-nm VCSEL [26] at ambient temperatures from 20 to 130 °C.

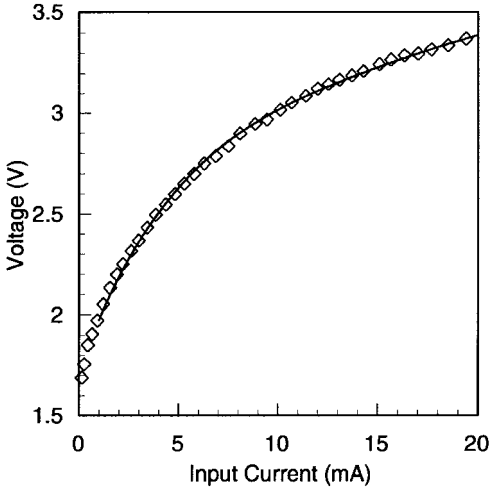

Fig. 3. Comparison of measured (data points) and simulated (lines) room-temperature IV curves for the device of Fig. 2.

The first device is an 863-nm bottom-emitting VCSEL with a 16-mm diameter, as reported by Ohiso *et al.* [26]. The device, grown on an $Al_{0.1}Ga_{0.9}As$ substrate, includes a Si-doped $Al_{0.15}Ga_{0.85}As$-AlAs, GaAs-$Al_{0.2}Ga_{0.8}As$ n-type DBR, six quantum wells, and a C-doped $Al_{0.15}Ga_{0.85}As$-$Al_{0.5}Ga_{0.5}As$-AlAs p-type DBR. In addition to presenting a family of LI curves over a 110 °C range of ambient temperatures, the authors also provide a room-temperature IV characteristic. We fit this device data using the following set of model parameters: $\eta_i = 1, \beta = 10^{-6}, \tau_n = 5$ ns, $k = 2.6 \times 10^{-8}$ W, $G_o = 1.6 \times 10^4\ \mathrm{s}^{-1}, N_o = 1.94 \times 10^7, \tau_p = 2.28$ ps, $R_{\mathrm{th}} = 2.6°$ C/mW, $a_0 = 1.246 \times 10^{-3}$ A, $a_1 = -2.545 \times 10^{-5}$ A/K, $a_2 = 2.908 \times 10^{-7}$ A/K^2, $a_3 = -2.531 \times 10^{-10}$ A/K^3, and $a_4 = 1.022 \times 10^{-12}$ A/K^4 where we have neglected gain saturation. Furthermore, for simplicity, we fit the IV data using a polynomial function of current

$$V = 1.721 + 275I - 2.439 \times 10^4 I^2 + 1.338 \times 10^6 I^3 - 4.154 \times 10^7 I^4 + 6.683 \times 10^8 I^5 - 4.296 \times 10^9 I^6. \tag{14}$$

As illustrated in Figs. 2 and 3, the simulation results generated with these parameters are in excellent agreement with experiment across nearly the full range of reported ambient temperatures, 20–130 °C. While the good fit of the IV data is to be expected from the use of (14), to the best of our knowledge, the level of agreement seen in Fig. 2 is as good as or better than any reported in the literature, including numerical models. One of the only potential drawbacks of the results is the thermal impedance value that we used, 2.6 °C/mW. Based on the reported temperature increase of 24 °C for an approximate operating point of 6 mA, 2.73 V, and 1.175 mW output power, the actual device thermal impedance is probably closer to 1.6 °C/mW. In all likelihood, the discrepancy arises out of the assumption that carrier-density-dependent effects such as spatial hole burning can be neglected in our model. By ignoring such effects, a higher value of thermal impedance is required to compensate for their absence and properly describe reduced efficiency at elevated currents. Nonetheless, the results are excellent.

The second device is an AlGaInP-based 683-nm selectively oxidized VCSEL with a 3 μm $\times$ 3 μm area, reported in [27] and [31] by Crawford *et al.* This device consists of compressively strained InGaP quantum wells, AlGaInP barrier and cladding layers, and AlGaAs graded DBR's. The authors provide both LI and IV curves over a 60 °C range of ambient temperatures. We fit the model of (2)–(6) to this experimental device data, this time using the following polynomial function to model the IV data as a function of current and temperature [19]

$$V = (0.829 - 1.007 \times 10^{-3} T + 6.594 \times 10^{-6} T^2 - 2.18 \times 10^{-8} T^3) \cdot (2.298 + 366.2I - 6.097 \times 10^4 I^2 + 6.76 \times 10^6 I^3). \tag{15}$$

The remaining model parameters are $\eta_i = 1, \beta = 10^{-6}, \tau_n = 5$ ns, $k = 2.6 \times 10^{-8}$ W, $G_o = 1.6 \times 10^4\ \mathrm{s}^{-1}, N_o = 1.654 \times 10^7, \tau_p = 2.064$ ps, $R_{\mathrm{th}} = 9.8$°C/mW, $a_0 = -2.734 \times 10^{-4}$ A, $a_1 = -2.125 \times 10^{-5}$ A/K, $a_2 = 1.837 \times 10^{-7}$ A/K^2, $a_3 = 3.183 \times 10^{-10}$ A/K^3, and $a_4 = 0$ A/K^4. We again neglected gain saturation. Note that because the LI data is fit via the parameters I_{tho} and η, there are not enough constraints within the data to uniquely determine all of the model parameters. Consequently, many of the values are the same as those generated for the Ohiso device.

Comparison of the simulated and experimental LI and IV curves is illustrated in Figs. 4 and 5. Our model shows excellent agreement in the ambient temperature range 25–60 °C. However, at higher ambient temperatures the simulated temperature effects are more pronounced than what the data suggests. In fact, the model was not able to match additional data at 85 °C; experimental measurements showed that the device lased at this temperature, while our model could not. The discrepancy at these higher ambient temperatures is most likely due to the omission of carrier-density-dependent effects in the model, as was the case with the earlier AlGaAs-

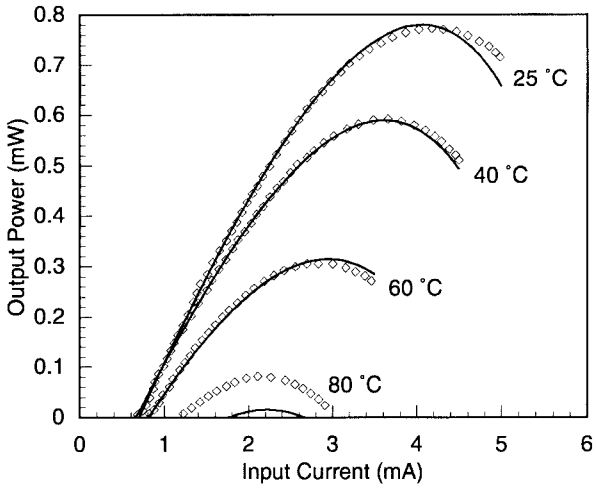

Fig. 4. Comparison of measured (data points) and simulated (lines) LI curves for an AlGaInP-based 683-nm VCSEL [27] at ambient temperatures from 25 to 80 °C.

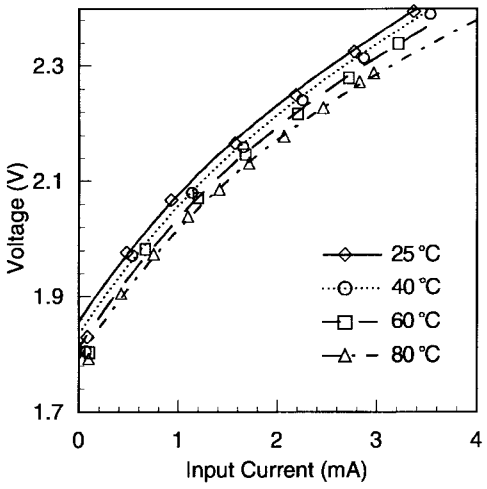

Fig. 5. Comparison of measured (data points) and simulated (lines) IV curves for the device of Fig. 4 at ambient temperatures from 25 to 80 °C.

based VCSEL. This is also evidenced by the high value of thermal impedance generated during parameter optimization, 9.8 °C/mW. This high value is necessary to compensate for the absence of other physical mechanisms in the model that would augment thermal effects. Furthermore, we did not improve the results by including additional terms in (2). In fact, we found that for this device, a single expression for the offset current as a function of temperature was not sufficient to model the temperature effects at all of the reported ambient temperatures. In other words, for any given value of thermal impedance $R_{\rm th}$, the threshold current at all reported ambient temperatures could not be modeled by a unique function of temperature. Again, this suggests the need for additional mechanisms in the model which contribute to the thermal behavior without being fully temperature-dependent themselves. Despite these limitations, however, we again observe that our model can be used as an accurate representation of the device over a useful range of operation.

The last device is a 3.1-μm diameter thin-oxide-apertured VCSEL reported by Thibeault *et al.* [28]. The device is

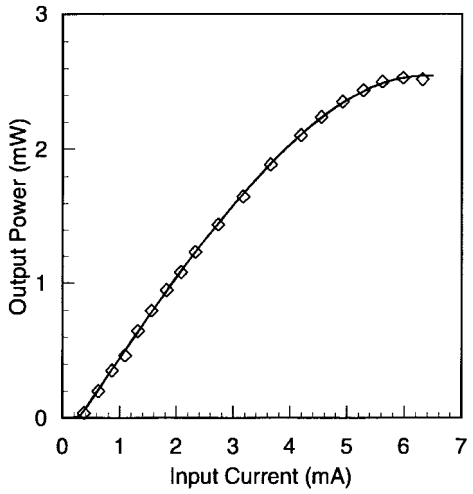

Fig. 6. Comparison of measured (data points) and simulated (lines) LI curves for an oxide-apertured VCSEL [28] at 23 °C.

composed of an $Al_{0.9}Ga_{0.1}As$-GaAs p-type DBR, three $In_{0.17}Ga_{0.83}As$-GaAs quantum wells, an $Al_{0.3}Ga_{0.7}As$ cavity, and an AlAs-GaAs n-type DBR. The authors present a single LI curve at a temperature of 23 °C. A plot of wall-plug efficiency is also provided from which IV data can be determined. Although LI data for only one ambient temperature are shown, the data clearly exhibit output power rollover at high currents. In addition, modulation responses (S_{21}) at five bias currents and a temperature of 22 °C are reported, thereby providing us with an opportunity to verify both the dc and small-signal capabilities of our model.

As with the first two devices, we were able to extract the following model parameters from the provided data: $\eta_i = 0.821, \beta = 2.68 \times 10^{-2}, \tau_n = 1.201$ ns, $k = 4.166 \times 10^{-8}$ W, $G_o = 8.486 \times 10^5$ s^{-1}, $N_o = 1.286 \times 10^6$, $\tau_p = 2.884$ ps, $\varepsilon = 3.888 \times 10^{-6}$, $R_{\rm th} = 0.896$°C/mW, $a_0 = 2.213 \times 10^{-3}$ A, $a_1 = -1.719 \times 10^{-4}$ A/K, $a_2 = 3.355 \times 10^{-6}$ A/K^2, $a_3 = 0$ A/K^3, and $a_4 = 0$ A/K^4. Meanwhile, the IV data at 23 °C was fit using the following simple diode-like relationship:

$$V = 149.8I + 0.9366 \ln\left(1 + \frac{I}{7.918 \times 10^{-5}}\right). \quad (16)$$

Also, because parasitic capacitance was considered to be a key limitation to the high-speed performance of this particular device [28], we included a 351-fF capacitor at the input of our model as depicted in Fig. 1. Figs. 6 and 7 illustrate the results of fitting our model to the experimental data.

As expected, Fig. 6 shows excellent agreement between the simulated and experimental LI data, with the thermal rollover near 6 mA clearly captured in simulation. Fig. 7 presents a comparison between experimental and simulated S_{21} data at bias currents of 0.5, 0.7, 1.0, 1.3, and 2.1 mA and a temperature of 22 °C. The simulation results were normalized to a low frequency value. As can be seen, there is good agreement between both sets of curves, including the values for the resonant frequencies, with the main discrepancies arising in the magnitudes of the resonant peaks themselves. Again, the inclusion of additional terms in (2) would not improve the result. However, future work will present a

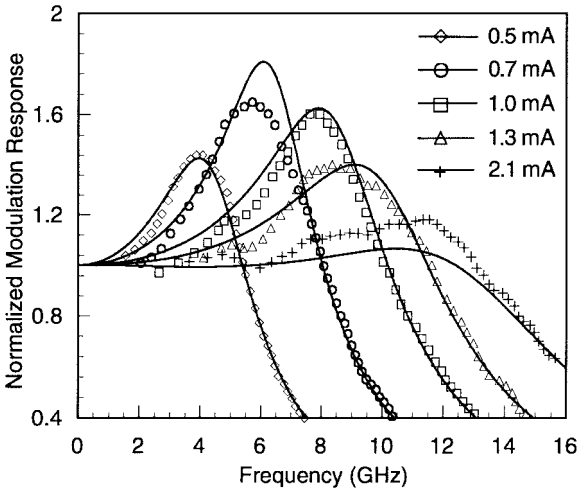

Fig. 7. Comparison of measured (data points) and simulated (lines) S_{21} curves for the device of Fig. 6 at 22 °C.

more comprehensive model that does. Nevertheless, the results are good given the simplicity of the rate equations used. Furthermore, they indicate that our approach allows thermal effects to be included in an extremely simple manner without sacrificing the ability to simulate VCSEL's under various regimes of operation, features which, as pointed out before, are very useful in the design and simulation of optoelectronic systems. It should be noted that because the ac curves in Fig. 7 are determined at operating currents below the device's rollover point, at currents near or beyond rollover the absence of true thermal-dependent mechanisms such as gain may limit the ability of the model to accurately simulate this device's small-signal and transient behavior. As discussed in Section II, however, a VCSEL will often be operated at currents below the rollover point. In this case, our model can be used to simulate the thermal limits of the device under dc operation, as well as non-dc behavior under more typical operating conditions, such as those discussed here.

IV. Conclusions

We have presented a simple rate-equation-based model of VCSEL thermal LI characteristics which utilizes an offset current to account for thermal effects. This model was implemented in two SPICE-like simulators, HSPICE and SABER. As we have seen, the model exhibits good agreement with experiment for numerous devices, suggesting its usefulness for describing a variety of VCSEL's. Furthermore, we were able to show using the device of Figs. 6–7 that our model is capable of simulating VCSEL's under non-dc operating regimes. Some discrepancies do exist, however, between the simulated and experimental results. In fitting the device of Figs. 2–3, we obtained a thermal impedance which was larger than the reported value. Furthermore, for the device of Figs. 4–5, we saw that the model over-predicts thermal effects at higher temperatures. In all likelihood, these errors are due to the assumptions that spatial hole burning can be neglected and that the slope efficiency is constant, the former being the predominant factor. In cases where these issues are critical, the model can be made more comprehensive by including thermally dependent gain [21], using a leakage current as a function of carrier number and temperature [19], and introducing spatial hole burning effects [19]. Such additions should also improve the non-dc capabilities of the model. However, even without any modifications, we have shown that the introduction of a thermal offset current into the standard rate equations provides an effective means for modeling experimental results without introducing excessive levels of complexity.

References

[1] K. Iga, F. Koyama, and S. Kinoshita,"Surface emitting semiconductor lasers," *IEEE J. Quantum Electron.*, vol. 24, pp. 1845–1855, Sept. 1988.
[2] C. J. Chang-Hasnain, J. P. Harbison, G. Hasnain, A. C. Von Lehmen, L. T. Florez, and N. G. Stoffel,"Dynamic, polarization, and transverse mode characteristics of vertical cavity surface emitting lasers," *IEEE J. Quantum Electron.*, vol. 27, pp. 1402–1409, June 1991.
[3] A. Valle, J. Sarma, and K. A. Shore,"Spatial holeburning effects on the dynamics of vertical cavity surface-emitting laser diodes," *IEEE J. Quantum Electron.*, vol. 31, pp. 1423–1431, Aug. 1995.
[4] ——,"Secondary pulsations driven by spatial hole burning in modulated vertical-cavity surface-emitting laser diodes," *J. Opt. Soc. Amer.*, pt. B, vol. 12, no. 9, pp. 1741–1746, 1995.
[5] T. E. Sale, J. S. Roberts, J. P. R. David, R. Grey, J. Woodhead, and P. N. Robson,"Temperature effects in VCSEL's," *Proc. SPIE*, vol. 3003, pp. 100–110, 1997.
[6] G. Hasnain, K. Tai, L. Yang, Y. H. Wang, R. J. Fischer, J. D. Wynn, B. Weir, N. K. Dutta, and A. Y. Cho,"Performance of gain-guided surface emitting lasers with semiconductor distributed Bragg reflectors," *IEEE J. Quantum Electron.*, vol. 27, no. 6, pp. 1377–1385, 1991.
[7] W. Nakwaski and M. Osinski,"Self-consistent thermal-electrical modeling of proton-implanted top-surface-emitting semiconductor lasers," *Proc. SPIE*, vol. 2146, pp. 365–387, 1994.
[8] R. Michalzik and K. J. Ebeling,"Modeling and design of proton-implanted ultralow-threshold vertical-cavity laser diodes," *IEEE J. Quantum Electron.*, vol. 29, pp. 1963–1974, June 1993.
[9] G. R. Hadley, K. L. Lear, M. E. Warren, K. D. Choquette, J. W. Scott, and S. W. Corzine,"Comprehensive numerical modeling of vertical-cavity surface-emitting lasers," *IEEE J. Quantum Electron.*, vol. 32, pp. 607–616, Apr. 1996.
[10] J. Piprek, H. Wenzel, and G. Sztefka,"Modeling thermal effects on the light vs. current characteristic of gain-guided vertical-cavity surface-emitting lasers," *IEEE Photon. Technol. Lett.*, vol. 6, pp. 139–142, Feb. 1994.
[11] L. J. Norton, F. Carney, N. Choi, C. K. Y. Chun, R. K. Denton, Jr., D. Diaz, J. Knapp, M. Meyering, C. Ngo, S. Planer, G. Raskin, E. Reyes, J. Sauvageau, D. B. Schwartz, S. G. Shook, J. Yoder, and Y. Wen,"OPTOBUS I: A production parallel fiber optical interconnect," in *Proc. IEEE Electron. Components and Technol. Conf.*, 1997, pp. 204–209.
[12] J. A. Neff,"VCSEL-based smart pixels for free-space optical interconnection," in *Proc. IEEE LEOS Annu. Meeting*, 1997, pp. 151–152.
[13] S. F. Yu, W. N. Wong, P. Shum, and E. H. Li,"Theoretical analysis of modulation response and second-order harmonic distortion in vertical-cavity surface-emitting lasers," *IEEE J. Quantum Electron.*, vol. 32, pp. 2139–2147, Dec. 1996.
[14] Y. Su, Y. Chang, and X. Chen,"Circuit model for studying temperature effects on vertical-cavity surface-emitting laser," in *Proc. IEEE LEOS Annu. Meeting*, 1996, vol. 1, pp. 215–216.
[15] T. Wipiejewski, M. G. Peters, B. J. Thibeault, D. B. Young, and L. A. Coldren,"Size-dependent output power saturation of vertical-cavity surface-emitting laser diodes," *IEEE Photon. Technol. Lett.*, vol. 8, no. 1, pp. 10–12, 1996.
[16] N. Bewtra, D. A. Suda, G. L. Tan, F. Chatenoud, and J. M. Xu,"Modeling of quantum-well lasers with electro-opto-thermal interaction," *IEEE J. Select. Topics Quantum Electron.*, vol. 1, no. 2, pp. 331–340, 1995.
[17] J. Piprek, D. I. Babic, and J. E. Bowers,"Simulation and analysis of 1.55 μm double-fused vertical-cavity lasers," *J. Appl. Phys.*, vol. 81, no. 8, pp. 3382–3390, 1997.
[18] W. Nakwaski,"Thermal aspects of efficient operation of vertical-cavity surface-emitting lasers," *Optic. Quantum Electron.*, vol. 28, pp. 335–352, 1996.
[19] J. W. Scott, R. S. Geels, S. W. Corzine, and L. A. Coldren,"Modeling temperature effects and spatial hole burning to optimize vertical-cavity

surface-emitting laser performance," *IEEE J. Quantum Electron.*, vol. 29, no. 5, pp. 1295–1308, 1993.
[20] G. P. Agrawal and N. K. Dutta, *Semiconductor Lasers, 2nd ed.* New York: Van Nostrand Reinhold, 1993.
[21] D. M. Byrne and B. A. Keating,"A laser diode model based on temperature dependent rate equations," *IEEE Photon. Technol. Lett.*, vol. 1, pp. 356–359, Nov. 1989.
[22] *HSPICE User's Manual*, Meta-Software, Inc., 1996.
[23] *MAST Language Reference Manual*, Analogy, Inc., 1996.
[24] P. V. Mena, S. M. Kang, and T. A. DeTemple,"Rate-equation-based laser models with a single solution regime," *J. Lightwave Technol.*, vol. 15, pp. 717–730, Apr. 1997.
[25] C. Lawrence, J. L. Zhou, and A. L. Tits,"Users' guide for CFSQP version 2.5: A C code for solving (large scale) constrained nonlinear (minimax) optimization problems, generating iterates satisfying all inequality constraints," Inst. Syst. Res., Univ. Maryland, College Park, Tech. Rep. TR-94-16r1, 1997.
[26] Y. Ohiso, K. Tateno, Y. Kohama, A. Wakatsuki, H. Tsunetsugu, and T. Kurokawa,"Flip-chip bonded 0.85-μm bottom-emitting vertical-cavity laser array on an AlGaAs substrate," *IEEE Photon. Technol. Lett.*, vol. 8, pp. 1115–1117, Sept. 1996.
[27] M. H. Crawford, K. D. Choquette, H. Q. Hou, R. J. Hickman, K. M. Geib, and B. E. Hammons,"Visible VCSELs: Recent advances and applications," in *Proc. 1997 Digest LEOS Summer Topical Meetings—Vertical-Cavity Lasers*, 1997, pp. 17–18.
[28] B. J. Thibeault, K. Bertilsson, E. R. Hegblom, E. Strzelecka, P. D. Floyd, R. Naone, and L. A. Coldren,"High-speed characteristics of low-optical loss oxide-apertured vertical-cavity lasers," *IEEE Photon. Technol. Lett.*, vol. 9, pp. 11–13, Jan. 1997.
[29] J. J. Morikuni and S. M. Kang, *Computer-Aided Design of Optoelectronic Integrated Circuits and Systems*. Upper Saddle River, NJ: Prentice Hall, 1997.
[30] M. Osinski and W. Nakwaski,"Thermal effects in vertical-cavity surface-emitting lasers," *Int. J. High Speed Electron. Syst.*, vol. 5, no. 4, pp. 667–730, 1994.
[31] M. H. Crawford, K. D. Choquette, R. J. Hickman, and K. M. Geib,"InAlGaP vertical cavity surface emitting lasers (VCSEL's): Processing and performance," in *Proc. Int. Conf. InP and Related Mater.*, 1997, pp. 32–35.

P. V. Mena (S'94–M'99), for a biography see p. 101 of the January 1999 issue of this JOURNAL.

J. J. Morikuni (S'91–M'95), for a photograph and biography see p. 101 of the January 1999 issue of this JOURNAL.

S.-M. Kang (S'73–M'75–SM'80–F'90), for a photograph and biography see p. 102 of the January 1999 issue of this JOURNAL.

A. V. Harton (M'92), for a photograph and biography see p. 101 of the January 1999 issue of this JOURNAL.

K. W. Wyatt, for a photograph and biography see p. 101 of the January 1999 issue of this JOURNAL.